Stationary nonequilibrium states by molecular dynamics. II. Newton's law

Carlo Trozzi and Giovanni Ciccotti
Dipartimento di Fisica "Guglielmo Marconi" e Gruppo Nazionale di Struttura della Materia del Consiglio Nazionale delle Ricerche, Piazzale Aldo Moro 2, I-00185 Roma, Italy
(Received 25 July 1983)

We present molecular-dynamics results for a dense Lennard-Jones fluid near the triple point subjected to the Couette flow. The method is based on the introduction of stochastic boundary conditions to simulate the contact with a moving thermal wall. The method allows the simulation of bulk properties of the system and the study of the local thermodynamical equilibrium. Furthermore, it gives a physical description of momentum and heat transfer near a Couette wall. We found that the shear viscosity depends on shear rate near the triple point (breakdown of Newton's law) while for a point far from the liquid-solid coexistence line there is no appreciable deviation from Newton's law. In the bulk region, where boundary effects are negligible, we found that the local thermodynamical equilibrium holds for all simulated shear rates (up to 1.14×10^{11} sec^{-1}). Moreover, we do not find any dependence on the number of particles used in the simulation. Last we compare the results for the shear-dependent shear viscosity with theoretical predictions for nonlinear behavior.

I. INTRODUCTION

In a previous paper[1] we studied the limits of validity of Fourier's law by introducing stochastic boundary conditions in molecular-dynamics (MD) computer experiments. There we showed how to use this technique to simulate stationary nonequilibrium states, in particular the contact of a MD system with thermal reservoir.

In this work the technique is implemented to simulate a Couette flow,[2] to calculate the shear viscosity of a dense fluid and to look for the breakdown of Newton's law, the linear phenomenological law for viscous transport.

In the past years equilibrium MD and several nonequilibrium MD techniques have been used to study viscous transport. They include the following:

(i) Computation of the Green-Kubo integral for the time-dependent stress-stress correlation function.[3–6]

(ii) Studies on models in which nonequilibrium boundary conditions are used to shear a MD system. These are the fluid walls model[7,8] and several versions of the homogeneous shear model.[9–14]

(iii) Solution of equations of motion subjected to an external perturbing field. These are the sinusoidal transverse force method[15,16] and the Doll's tensor Hamiltonian method.[17] Its use can require particular boundary conditions as in (ii).

The techniques in (ii) and (iii) can be used to compute the direct response of the system. Alternatively they can be used together with the differential method.[18,19] In this last the response induced by a perturbing field or boundary conditions is calculated as the difference between the variable conjugate to the perturbation in perturbed and unperturbed phase-space trajectories. The success of the method rests on the cancellation of large thermal fluctuations as a result of the differential technique. The homogeneous shear model, replacing the constant perturbing field by a time-dependent sinusoidal one, has been used to compute a frequency-dependent shear viscosity and to obtain from its low-frequency behavior the long-time tail of the stress-stress correlation function.[13]

The main results of the computer experiments are as follows. In the equilibrium MD simulations near the triple point[3–5] the stress-stress correlation function shows a long-time tail and the results depend on particle number. Moreover, the computed shear viscosity for the largest system is $\sim20\%$ greater than the experimental one. For a state far away from this region these effects are less important.[6] In the nonequilibrium MD simulations the results show an applied perturbation-dependent shear viscosity, decreasing with increasing perturbation. Some models[7,8] and some results (for hard-spheres systems) in the homogeneous shear model[11] show also a dependence on particle number. This dependence is opposite to that in equilibrium MD. In the hard-spheres simulation,[11] if an N^{-1} dependence is assumed, the infinite size shear viscosities are the same, within the statistical errors, for all shear rates. Moreover, in some work[13,14,16] the pressure and the internal energy also show applied shear dependence with the consequent breakdown of local thermodynamical equilibrium.

There are two theories which attempt to describe the breakdown of Newton's law and of the local equilibrium hypothesis for increasing applied perturbation. They are the Kawasaki-Gunton-Yamada (KGY) mode-mode coupling theory and the Quentrec (Q) local-order theory. The MD results have been explained in some work within the KGY theory. However the numerical parameters obtained by MD are very different from the theoretical estimates.

The KGY predictions[20,21] are

$$\eta(\omega)=\eta_0-A\omega^{1/2}\ ,$$

$$P(\omega)=P_0+B\omega^{3/2}\ ,$$

$$\sigma_1(\omega)=\Pi_{yy}(\omega)-\Pi_{xx}(\omega)=C_1\omega^{3/2} ,$$

$$\sigma_2(\omega)=\Pi_{zz}(\omega)-\Pi_{xx}(\omega)=C_2\omega^{3/2} ,$$

with ω the shear rate, η the shear viscosity, P the pressure, and Π_{ij} the i,j component of the stress tensor. From now on we define the shear rate ω as $\omega=\partial v_y/\partial x$ and we write the Newton law as $\Pi_{xy}=\eta\omega$.

The Q predictions[22,23] are

$$\eta(\omega)=\eta_0\left[1-\frac{R\omega^2}{\Gamma^2+\omega^2}\right] ,$$

$$\sigma_1(\omega)=2\eta_0\frac{R\Gamma\omega^2}{\Gamma^2+\omega^2} ,$$

$$\sigma_2(\omega)=\tfrac{1}{2}\sigma_1(\omega) .$$

Moreover, Hanley and Evans introduce[24] the relation

$$U(\omega)=U_0+D\omega^{3/2}$$

to explain the dependence of the internal potential energy U on the shear rate found in their computer experiments.

In this work all these effects are studied for a Lennard-Jones fluid. The main conclusion we can draw within the precision of our calculation is that, near the triple point, there is a dependence of the shear viscosity on the applied perturbation but no breakdown of the local equilibrium hypothesis. Also we do not find any dependence on particle number.

In Sec. II we give details of the model with stochastic boundary conditions. In Sec. III we recall the microscopic expressions for the local properties. In Sec. IV we describe the computer experiments and study in detail the boundary mechanism and the boundary effects. In Sec. V we analyze the validity of local equilibrium hypothesis and present the results for shear viscosity and their interpretation. Section VI is devoted to some concluding remarks.

II. THE MODEL

We consider a system of N particles enclosed in a parallelepiped Λ of sides L_x,L_y,L_z $(L_y=L_z<L_x)$ interacting through a two-body potential of the Lennard-Jones type. As in Ref. 25 the potential is truncated at a certain distance R_c. The values chosen for R_c are nearly the largest consistent with the minimum image convention. They are listed in Table I. The units are σ for length, ϵ for energy, and $\tau=(m\sigma^2/48\epsilon)^{1/2}$ for time. For argon, $\sigma=3.405$ Å, $\epsilon=119.8k_B$, $\tau=3.112\times10^{-13}$ sec.

A Couette flow is produced in a fluid enclosed by two parallel walls in uniform motion with a relative velocity different from zero. The system is enclosed between two y-z planes at a distance L_x. The lower wall (the upper wall) moves with a velocity $+V$ $(-V)$ in the y direction. It is assumed that (i) fluid velocity at the walls is equal to the velocity of the wall, i.e., there is no slip, and (ii) the transport coefficients are constant in the bulk. The slip at the wall is discussed in Sec. IV.

The Navier-Stokes equations give for the bulk velocity a linear profile

$$v_y(x)=\frac{2V}{L_x}x\equiv\omega_0 x . \tag{1}$$

The phenomenological Newton's law assumes that the x,y component of the stress tensor $\overleftrightarrow{\Pi}$ is proportional to the applied gradient

$$\Pi_{xy}=\eta\frac{\partial v_y}{\partial x}=\eta\omega_0 , \tag{2}$$

where η is the shear viscosity coefficient.

Moreover, if the walls are kept at constant temperature T_w and there is no temperature drop at the walls (the temperature drop is discussed in Sec. IV) the heat hydrodynamical equation gives the parabolic temperature profile

$$T(x)=T_w+\frac{\eta\omega_0^2}{2\lambda}\left[\frac{L^2}{4}-x^2\right] , \tag{3}$$

where λ is the thermal conductivity coefficient.

Stochastic boundary conditions are used to simulate Couette flow. The boundary conditions are periodic in the y,z directions, while in the x direction Λ is bounded by stochastic walls realized in the way described below. The equations of motion to be integrated are[1]

$$m\frac{d^2\vec{r}_i}{dt^2}=-\sum_{j\,(\neq i)}\vec{\nabla}_{\vec{r}_i}u(r_{ij})+\vec{f}_w(\vec{r}_i) , \quad i=1,\ldots,N \tag{4}$$

where $\vec{f}_w(\vec{r})$ is an impulsive stochastic force acting only when the particle hits a stochastic wall. Its effect is to reenter the particle into the box at the same place, but with y and z velocities sampled from a Maxwellian distribution at the wall temperature T_w, mean y-component V_w and mean z-component zero

TABLE I. List of thermodynamic states and model parameters. ρ, number density; T, temperature; N, number of particles; m, number of different shear rates imposed to the given state; R_c, potential cutoff; N_L,V_L,l, number, volume, and thickness of layers, respectively.

ρ	T	N	m	R_c	N_L	V_L	l
0.75	0.8752	384	1	3.0	12	42.7	0.8736
0.8442	0.722	180	4	2.5	10	21.3	0.8398
0.8442	0.722	384	6	3.0	12	37.9	0.8398

$$\Phi(v_y)=(2\pi m k_B T_w)^{-1/2}\exp\left[-\frac{m(v_y-V_w)^2}{2k_B T_w}\right], \quad (5)$$

$$\Phi(v_z)=(2\pi m k_B T_w)^{-1/2}\exp\left[-\frac{mv_z^2}{2k_B T_w}\right], \quad (6)$$

$V_w=+V$ on the right wall and $V_w=-V$ on the left wall; in the x direction the velocity component is sampled from

$$\Phi(v_x)=\frac{m}{k_B T_w}v_x\exp\left[-\frac{mv_x^2}{2k_B T_w}\right]. \quad (7)$$

The set of coupled differential equations (4) is integrated with the central difference algorithm.[25] The value of the time step in our computations is always $h=0.032$. The procedure used to take into account the stochastic impulsive force $\vec{f}_w$ has been already described.[1]

The difference between the ideal mechanism and its numerical implementation can give rise to errors in the integration of equations of motion. In particular, for high boundary velocities or at high temperatures, a particle can be moved in the nearest neighborhood of another particle. In such a case the high value of repulsive potential energy between the particles could affect the integration step. We checked the validity of our procedure by monitoring the energy of a canonical ensemble at very high temperature [$T=2.9$, corresponding to $(\langle v^2\rangle)^{1/2}=0.25$]. This is the highest value of the boundary velocity for Couette flow in our computer experiment. The variation of the instantaneous total energy of the system, corrected for the contribution of collision with the stochastic walls, is ten times greater than the small variation corresponding to the microcanonical ensemble.

The main features of the present model can be summarized as follows.

(i) The velocity perturbation is confined to the walls; the dynamical evolution of the bulk is not altered.

(ii) The thermal mechanism acts only at the walls without any scaling of the internal kinetic energy.

(iii) The velocity and temperature of the walls have a precise statistical meaning.

(iv) The model affords a physical description of Couette flow which can be compared with the analytical solution of Navier-Stokes and heat equations.

Because in this model the boundary conditions in the x direction are not periodic, there are no "images" of particles beyond the stochastic walls. Thus surface effects affect some "local" thermodynamic properties. Since the size of a typical MD system is small, these effects could be relevant. However, it is possible to control such effects as we shall see later (Secs. IV and V).

III. STATISTICAL MECHANICAL DEFINITION OF LOCAL PROPERTIES

The thermodynamic study must be performed from a local point of view to monitor the gradients. For this purpose the system has been divided into N_L layers of equal size parallel to the stochastic walls. In each layer we computed the smoothed values of local density, velocity, temperature, internal potential energy, pressure, and stress tensor. The computation of these values goes as follows.[1] The local value of an observable A at point $\vec{r}$ is

$$A(\vec{r})=\langle A(\vec{r}\,|\,\{\vec{r}_i,\vec{p}_i\}_{i=1}^{i=N})\rangle , \quad (8)$$

where the quantity to be averaged can be written in general as the sum over the particles of the corresponding property defined for each particle. Thus

$$A(\vec{r}\,|\,\{\vec{r}_i,\vec{p}_i\}_{i=1}^{i=N})=\sum_{i=1}^{N}A_i(\{\vec{r}_j,\vec{p}_j\}_{j=1}^{j=N})\delta(\vec{r}-\vec{r}_i) \quad (9)$$

where A_i is equal to (i) 1 for density field $\rho(\vec{r})$, (ii) $[3k_B\rho(\vec{r})]^{-1}m[\vec{v}_i-\langle\vec{v}(\vec{r})\rangle]^2$ for temperature field $T(\vec{r})$, (iii) $[\rho(\vec{r})]^{-1}\vec{v}_i$ for the velocity field $\vec{v}(\vec{r})$, and (iv) $[2\rho(\vec{r})]^{-1}\sum_{j(\neq i)}u(r_{ij})$, where $\vec{r}_{ij}=\vec{r}_i-\vec{r}_j$ and $u(r_{ij})$ is the pair potential, for the internal potential energy field $U(\vec{r})$.

For the stress tensor $\overleftrightarrow{\Pi}(\vec{r})$ one has

$$\overleftrightarrow{A}_i=-m[\vec{v}_i-\langle\vec{v}(\vec{r})\rangle][\vec{v}_i-\langle\vec{v}(\vec{r})\rangle]+\tfrac{1}{2}\sum_{j(\neq i)}\frac{\vec{r}_{ij}\vec{r}_{ij}}{r_{ij}}u'(r_{ij}) . \quad (10)$$

The pressure field $P(\vec{r})$ is equal to minus one-third the trace of the stress tensor.

The value of a given observable in layer σ ($\sigma=1,\ldots,N_L$) is finally

$$A_\sigma(\{\vec{r}_i,\vec{p}_i\}_{i=1}^{i=N})=\frac{1}{V_L(\sigma)}\int_{V_L(\sigma)}d\vec{r}\,A(\vec{r}\,|\,\{\vec{r}_i,\vec{p}_i\}_{i=1}^{i=N}) , \quad (11)$$

where $V_L(\sigma)$ is the volume of layer σ. The smoothed values of thermodynamic fields in each layer are then obtained by averaging in time the corresponding observables (9). V_L is chosen by a compromise between two opposite requirements: (i) the local thermodynamic analysis suggests the use of a small V_L, and (ii) the number of particles in each layer should be high to improve statistics.

As the potential is cut off at R_c the potential terms in internal energy and stress tensor must be corrected to take into account long-range contributions. The potential terms can be written as[26]

$$\overleftrightarrow{\Pi}^p(\vec{r})=\frac{\rho(\vec{r})}{2}\int\frac{\vec{R}\vec{R}}{R}u'(r)\rho(\vec{r}+\vec{R})g(\vec{r},\vec{R})d\vec{R} ,$$

$$U(\vec{r})=\tfrac{1}{2}\int u(\vec{R})\rho(\vec{r}+\vec{R})g(\vec{r},\vec{R})d\vec{R} .$$

Under the hypothesis of slowly varying density, $\rho(\vec{r}+\vec{R})\simeq\rho(\vec{r})$ and $g(\vec{r},\vec{R})\simeq g(\vec{R})$. Moreover, for $R>R_c$, $g(\vec{R})\simeq 1$. Neglecting the term R^{-12} of the Lennard-Jones potential, one obtains in reduced units

$$\Pi_{\alpha\beta}(\vec{r}\,|\,R>R_c)=\begin{cases}0, & \alpha\neq\beta\\ \dfrac{16\pi}{3R_c^3}[\rho(\vec{r})]^2, & \alpha=\beta\end{cases}$$

$$U(\vec{r}\,|\,R>R_c)=-\frac{8\pi}{3R_c^3}\rho(\vec{r}) .$$

The computation of thermodynamical fields allows us to test the validity of the local-equilibrium hypothesis. The weak form of the latter we use is

$$\Phi(\vec{r})=\Phi(X(\vec{r}),Y(\vec{r}))\ ,$$

where $X(\vec{r})$ and $Y(\vec{r})$ are two independent thermodynamical variables. In our simulations the pressure should be constant through the bulk while density and temperature vary from layer to layer. Therefore, we compared the experimental equation of state $\rho_{\text{expt}}=\rho(T(\vec{r}),P)$ and the internal potential energy $U=U(T(\vec{r}),P)$, obtained by standard equilibrium MD,[25] with the computed $\rho(\vec{r})$ and $U(\vec{r})$, respectively. The results confirm the validity of the weak local equilibrium hypothesis and are discussed in Sec. V.

IV. COMPUTER EXPERIMENT

The first part of the computer experiment consists in the realization of a chosen thermodynamic equilibrium state at $T=T_{\text{eq}}$. In this stage the system has the usual periodic boundary conditions[25] and constant total energy. At time $t=t^*$ the two yz boundaries are transformed into stochastic Couette walls while the other boundaries remain periodic.

The two thermodynamical states chosen as starting points for setting up Couette flow are given in Table I. The point at higher density is near the triple point of argon and has been extensively studied while the other has been used only to test the present model. The parameters of our computer experiments are given in Table I.

A. Shear rate limitations

The Reynold number criterion for laminar flow is[2]

$$R=\frac{2m\rho V_w L_x}{\eta}<R_{\text{crit}}$$

where R_{crit} between 10^3–10^4. Our V_w are always much below this turbulence threshold.

The applied shear rate must produce average values of the stress tensor greater than its spontaneous fluctuations. These last can be measured by monitoring the fluctuations of the unperturbed components of the stress tensor Π_{xz} and Π_{yz}. Another limit to the shear rate is due to heat effects in the bulk fluid; this upper limit is attained when, to obtain a prefixed stationary bulk temperature, the boundary temperature must be put to zero.

B. Toward the stationary state

The relaxation time needed to establish the stationary nonequilibrium state is very long if one starts from the equilibrium state. In a test run ($\rho=0.75$) we applied a boundary velocity $V_w=\pm 0.25$ and a boundary temperature $T_w=0.8752$ to the system in equilibrium.

The system enters in a transient stage where the local values of thermodynamic quantities are time dependent. This time evolution can be observed by taking averages over short time intervals (250 time steps). A linear profile of the velocity field is reached in a few time steps (~ 1000), while a stationary linear profile requires more than 4000 time steps. Moreover, the temperature increases with time. The stochastic walls give ordered kinetic energy to the system. This energy is used both to create a profile in the velocity field and to increase the local temperature by dissipation.

To reduce the relaxation time we selected a new starting point given by equilibrium configuration for positions and local Maxwell distributions for velocities. The velocity of any particle in layer σ is sampled from

$$f(\vec{v}_\sigma)=(2\pi m k_B T_\sigma)^{-1/2}\exp\left[-\frac{m(\vec{v}-\vec{V}_\sigma)^2}{2k_B T_\sigma}\right]\ , \tag{12}$$

where [see Eqs. (1) and (3)]

$$\vec{V}_\sigma=(0,\omega x_\sigma,0)\ ,$$

$$T_\sigma=T_w+\frac{\eta\omega^2}{2\lambda}\left[\frac{L_x^2}{4}-x_\sigma^2\right]\ ,$$

with x_σ being the coordinate of the center of the layer to which the particles belongs, and η and λ the experimental values of the shear viscosity and thermal conductivity. The temperature at the walls T_w is such that $(1/N_L)\sum_\sigma T_\sigma$ is equal to the temperature of the initial equilibrium state.

These initial conditions ensure a fast relaxation to a stationary state (of the order of 2000 time steps). However, the relaxed linear profile is smaller than the one imposed. This is caused by slip and temperature drop at the walls, as we shall see. The mean temperature reaches a value greater than the initial one due to some residual dissipation.

To reduce the temperature increase, the velocities are sampled from Eq. (12) as explained but the walls are assigned a temperature $T_w'=\alpha T_w$, and a velocity $V_w'=\beta V_w$. The parameters $\alpha<1$ and $\beta>1$ are numbers estimated in an empirical way to improve the efficiency in the choice of the final thermodynamical state. The choice of α and β could be made less arbitrary by considering the effects of slip and temperature drop.

C. Slip and temperature drop at the walls

When the stationary state is reached the velocity gradient of the system is lower than the one imposed at the boundaries. The velocity profile of the internal layers is linear although the boundary layers are usually outside the linear profile. Their velocity is between the wall velocity and that obtained by extrapolating at the wall the internal profile (Fig. 1).

Thus the results are characterized by the following parameters.

(i) The slope obtained by linear least-squares fit through the internal layers (shear rate)

$$\omega=\frac{\partial v_y(x)}{\partial x}\ . \tag{13}$$

(ii) The slip at the walls defined as

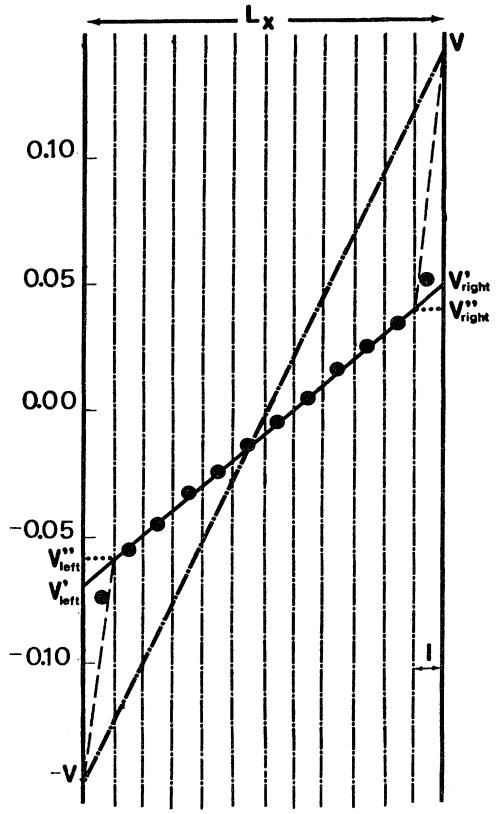

FIG. 1. Imposed and obtained velocity profiles. L_x distance between stochastic walls, l thickness of atomic layers, V velocity of the walls, ● local velocity V_σ ($\sigma=1,\ldots,N_L$), —·—·—· applied gradient, —— linear least-squares profile through N_L-2 internal layers, — — — local gradient across the outermost layers. Average density $\rho=0.8442$ and particle number $N=384$.

$$\Delta V_{\text{left}}=V'_{\text{left}}+V\ ,$$
$$\Delta V_{\text{right}}=V-V'_{\text{right}}\ , \tag{14}$$

where V'_{left} and V'_{right} are the velocities extrapolated at the walls of the internal profile.

(iii) The local gradient at the walls defined as

$$\nabla V_{\text{left}}=(V''_{\text{left}}+V)/l\ ,$$
$$\nabla V_{\text{right}}=(V-V''_{\text{right}})/l\ ,$$

where V''_{left} and V''_{right} are the velocities at the border of the region in which the velocity profile is linear and l is the layers thickness.

The velocity slip is a well-known effect in the kinetic theory of gases.[27] A molecule colliding with a solid surface may not acquire the velocity and energy corresponding to the state of the surface. Some molecules are elastically reflected, the rest enter the material and later leave it with the temperature and velocity of the wall. For a system in equilibrium this effect is immaterial because the wall and the system have the same mean velocity (namely, zero) and the same temperature. Under nonequilibrium conditions this effect can become important. If there exists a relative motion between the gas and the wall, velocity is transferred between them. If there exists a temperature difference, heat or energy is transferred. If, on the average, a molecule does not acquire the velocity of the wall in a collision, one says that there is "slip." If, on the average, a molecule does not acquire the energy corresponding to the temperature of the wall in a collision, one can say that there is "temperature drop." Therefore, under slip conditions the velocity of the molecules near the wall is different from that of the wall. The same is true under temperature-drop conditions. Since these are collisional effects they are important only in a region of the order of the mean free path.

In our computer experiments the fluid is dense and the concept of mean free path is not clear. Nevertheless we can define an effective mean free path corresponding approximately to the thickness of an atomic layer. Indeed the region near the Couette walls, where there is slip, has a range of the order of our layers.

Following Ref. 27 we can write, after some elementary substitutions,

$$\Delta V_i=\xi\frac{1}{\rho_i T_i^{1/2}}\nabla V_i,\quad i=\text{left, right}$$

where the coefficient ξ depends on the state of the fluid through the shear viscosity coefficient and the fraction of molecules striking the Couette wall which enter the material and leave it with the temperature and mean velocity of the wall.

In Fig. 2 we show the value of ΔV_i as a function of $\nabla V_i/\rho_i T_i^{1/2}$ (ρ_i and T_i are the density and temperature, respectively, of boundary layers) for all shear rates at average density $\rho=0.8442$ and number of particles 180 and 384. We have a linear pattern and no dependence on particle number. The linear least-squares fit gives for all data the value $\xi=0.45\pm0.04$. If we consider only data with the same particle number we have $\xi=0.48\pm0.05$ for 108 particles and $\xi=0.42\pm0.04$ for 384 particles, i.e., no appreciable difference.

For higher gradients, in which also the parabolic temperature profile is appreciable, there is also a temperature drop at the walls (Fig. 3). Proceeding in a similar way we

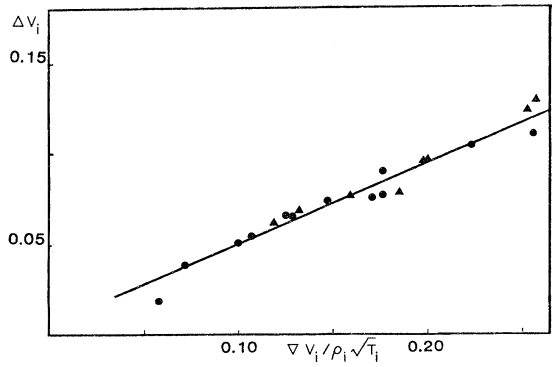

FIG. 2. Velocity slip ΔV_i as a function of $\nabla V_i/\rho_i T_i^{1/2}$. ∇V_i local gradient, ρ_i local density, and T_i local temperature near the wall. Average density $\rho=0.8442$; ●, $N=384$; ▲, $N=180$.

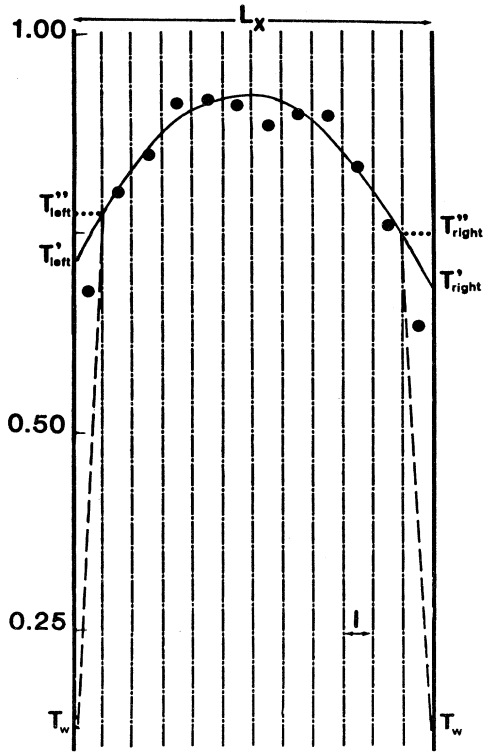

FIG. 3. Temperature profile. L_x distance betwen stochastic walls, l thickness of atomic layers, T_w wall temperature, ● local temperature T_σ ($\sigma=1,\ldots,N_1$), —— parabolic least-squares profile through N_L-2 internal layers, — — — local gradient across the outermost layers. Average density $\rho=0.8442$ and particle number $N=384$.

define (i) the temperature drop

$$\Delta T_i = T_i' - T_w, \quad i=\text{left, right}$$

where T_i' is the extrapolation of the internal profile at the walls, and (ii) the local gradients at the walls

$$\nabla T_i = (T_i'' - T_w)/l, \quad i=\text{left, right}$$

where T_i'' is the temperature at the border of the region in which the temperature profile is parabolic. Then[27]

$$\Delta T_i = \gamma \frac{1}{\rho_i T_i^{1/2}} \nabla T_i, \quad i=\text{left, right}$$

where $\gamma \propto \xi$.

In Fig. 4 we show the value of ΔT_i as a function of

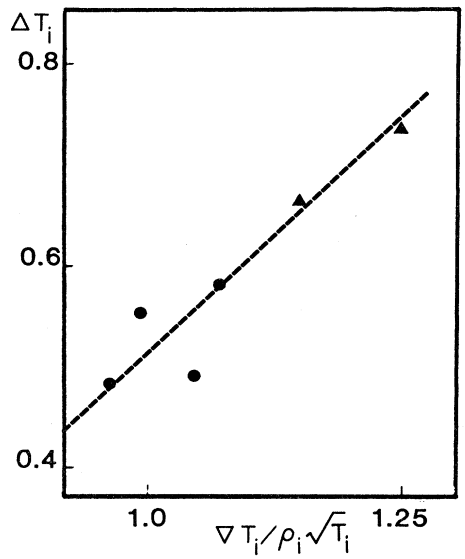

FIG. 4. Temperature drop ΔT_i as a function of $\nabla T_i/\rho_i T_i^{1/2}$. ∇T_i local gradient, ρ_i local density and T_i local temperature near the wall. Average density $\rho=0.8442$, ●, $N=384$, ▲, $N=180$.

$\nabla T_i/\rho_i T_i^{1/2}$ for the highest gradients, average density $\rho=0.8442$ and number of particles 180 and 384. We have a fairly linear profile and no appreciable dependence on particle number. The linear least-squares fit gives the value $\gamma=0.87\pm0.20$.

The thermal conductivity coefficient λ may be estimated from the fit of the temperature profile, see Eq. (3), using calculated shear rate and shear viscosity. The value of λ is affected by a standard error which is given by the combined errors of (i) the quadratic coefficient of Eq. (3), $a=\eta\omega^2/2\lambda$, (ii) the calculated shear viscosity η (see Sec. V), and (iii) the actual shear rate ω

$$s_\lambda = \left[\frac{\omega^4}{4a^2}s_\eta^2 + \frac{\eta^2\omega^4}{4a^4}s_a^2 + \frac{\eta^2\omega^2}{a^2}s_\omega^2\right]^{1/2}.$$

The results (Table II) obtained for thermal conductivity are consistent with experimental data.[28]

V. RESULTS

A. Local thermodynamical equilibrium

A local thermodynamical analysis of the simulated stationary states has been performed to check the validity of

TABLE II. Thermal conductivity estimated from temperature profiles. P, pressure; T, temperature; N, particle number; λ, thermal conductivity; s_λ, standard deviation of thermal conductivity; λ_{expt}, experimental data from Ref. 28.

P	T	N	$\lambda\pm s_\lambda$	λ_{expt}
1.0147	1.1500	384	0.85±0.15	0.79
0.0405	0.6594	384	0.70±0.15	1.08
0.8412	0.8310	384	1.04±0.15	1.03
0.6975	0.7977	180	1.61±0.37	1.04

the weak local equilibrium hypothesis. We compared the layer density ρ_σ ($\sigma=1,\ldots,N_L$) and the internal potential energy U_σ with the experimental density, $\rho_{\text{expt}}=\rho(T_\sigma,P)$, and the equilibrium MD internal potential energy, $U_{\text{eq MD}}=U(T_\sigma,P)$, respectively.

We report in Table III the results for the most critical cases, i.e., the highest shear rates, for the two different system studied ($N=180$ and 384, respectively). Pressures are the averages of the N_L-4 internal layers computed as shown in Sec. III. We excluded the local pressures of the four outermost layers from the average because they fall systematically outside the range of the internal values. Indeed, the microscopic expression used to compute the pressure is valid only in the bulk and does not apply near the walls, where the force field on the particles is altered by the absence of images beyond the walls. This effect, however, does not extend farther than two layers; therefore, the bulk value of the pressure can be obtained from the remaining N_L-4 internal layers.

The agreement between experimental versus computed densities and equilibrium MD versus computed internal potential energies is satisfactory and makes one confident in the validity of the weak local equilibrium hypothesis. The only relevant deviations are, as expected, two boundary layers for densities (one for each side) and four boundary layers for internal potential energies. These deviations, due to the absence of images, affect configurational quantities like local density, internal potential energy, and stress tensor, but are essentially irrelevant for kinetic quantities. For internal potential energy as for pressure the microscopic expression is significant in the bulk but not near the walls. The inhomogeneity of the density in the boundary layers depends, as we shall see later, from the bulk compressibility factor. From Table III it is apparent that for dense fluids near the triple point the local equilibrium hypothesis can be confirmed at least up to shear rate of the order of $0.035(48\epsilon/m\sigma^2)^{1/2}$.

B. Newton's law

All simulated stationary states have a fairly linear velocity profile through the N_L-2 internal layers, while the velocities of the two boundary layers are outside the profile due to slip at the walls. Thus we define the shear rate ω by doing a linear regression through the N_L-2 internal layers velocities. The stress tensor off-diagonal component Π_{xy} has been calculated using Eqs. (8)—(11) with the further average

$$\overline{\Pi}_{xy}=\frac{1}{N_L-2}\sum_{2}^{N_L-1}\langle\Pi_{xy}^{\sigma}\rangle\ ,$$

$\langle\Pi_{xy}^{\sigma}\rangle$ being the local stress in layer σ. As usual two

TABLE III. Local equilibrium test. T_σ and ρ_σ local temperature and density, respectively; ρ_{expt}, interpolated and/or extrapolated experimental data from Ref. 28 for density corresponding to (T_σ,P); Δ_ρ, percentage difference between computed and experimental density; U_σ, local internal potential energy; $U_{\text{eq MD}}$, interpolated or extrapolated equilibrium molecular dynamics (eq MD) data from Ref. 25 for internal energy corresponding to (T_σ,ρ_σ); Δ_U, percentage difference between computed and eq MD internal potential energy.

Layer	T_σ	ρ_σ	ρ_{expt}	Δ_ρ (%)	U_σ	$U_{\text{eq MD}}$	Δ_u (%)
			(a) $P=0.8412$, $N=384$, $\omega=0.0345$				
1	0.675	0.8770	0.9016	2.7	−4.06	−6.34	36.0
2	0.802	0.8665	0.8559	−1.2	−5.54	−6.07	8.7
3	0.850	0.8471	0.8386	−1.0	−5.78	−5.95	2.9
4	0.913	0.8309	0.8160	−1.8	−5.71	−5.79	1.4
5	0.917	0.7984	0.8145	2.0	−5.67	−5.58	1.6
6	0.911	0.8133	0.8167	0.4	−5.65	−5.68	0.6
7	0.833	0.8193	0.8268	0.9	−5.69	−5.75	1.0
8	0.899	0.8070	0.8240	1.7	−5.74	−5.66	−1.4
9	0.896	0.8143	0.8210	0.9	−5.81	−5.70	−2.0
10	0.830	0.8679	0.8458	−2.6	−5.87	−6.03	2.7
11	0.759	0.8781	0.8714	−0.8	−5.71	−6.19	7.8
12	0.633	0.9108	0.9168	0.6	−4.20	−6.69	37.1
			(b) $P=0.6975$, $N=180$, $\omega=0.0354$				
1	0.732	0.8496	0.8725	2.6	−3.89	−6.10	36.2
2	0.830	0.8319	0.8368	0.6	−5.37	−5.88	8.7
3	0.858	0.8437	0.8267	−2.1	−5.72	−5.95	3.9
4	0.876	0.8285	0.8201	−1.0	−5.80	−5.81	0.2
5	0.843	0.8146	0.8321	2.1	−5.80	−5.76	−0.7
6	0.837	0.8208	0.8343	1.6	−5.83	−5.80	−0.5
7	0.830	0.8339	0.8368	0.4	−5.88	−5.89	0.2
8	0.793	0.8628	0.8503	−1.5	−5.86	−6.07	3.5
9	0.759	0.8727	0.8626	−1.2	−5.60	−6.12	8.5
10	0.619	0.8835	0.9135	3.3	−4.09	−6.50	37.1

TABLE IV. Results for the shear viscosity. ω, shear rate; ρ_B, bulk density; T, temperature; P pressure; $P/\rho_B kT$, compressibility factor; N, particle number ; η, computer shear viscosity and s_η standard error; η_{expt}, experimental value from Ref. 28; η^{ad}, shear viscosity adjusted to a temperature $T_0=0.722$, and density $\rho=0.8442$. The corresponding experimental result is $\eta^{\text{ad}}_{\text{expt}}=22.75$ (Ref. 28). For the point at negative pressure the experimental result is taken at zero pressure.

ω	ρ_B	T	P	$P/\rho_B kT$	N	$\eta\pm s_\eta$	η_{expt}	η^{ad}
0.032	0.7438	1.1500	1.0147	1.19	384	11.27±0.36	11.07	
0.0032	0.8568	0.6858	0.1773	0.30	384	25.50±2.42	27.25	21.29
0.0053	0.8624	0.6295	0.0066	0.012	180	28.62±2.97	32.11	20.28
0.0068	0.8529	0.7080	0.3173	0.53	384	24.09±2.36	26.92	20.36
0.0082	0.8499	0.7096	0.1180	0.20	180	24.45±1.24	23.38	23.79
0.0092	0.8523	0.6394	−0.2093	−0.39	180	25.32±1.59	30.27	19.03
0.0094	0.8484	0.7365	0.4414	0.71	384	19.69±1.23	25.52	17.55
0.0119	0.8499	0.7326	0.3768	0.60	384	19.17±1.22	24.88	17.53
0.0185	0.8538	0.6594	0.0405	0.07	384	17.70±0.61	28.01	14.38
0.0345	0.8343	0.8307	0.8412	1.21	384	16.14±0.65	23.09	15.90
0.0354	0.8368	0.7977	0.6975	1.04	180	16.21±0.91	23.97	15.39

outermost layers are excluded.

The shear viscosity η is given by Newton's law, Eq. (2). Its standard error is the combined error on $\overline{\Pi}_{xy}$ and ω

$$s_\eta=\left[\frac{1}{\omega^2}s^2_{\overline{\Pi}_{xy}}+\frac{(\overline{\Pi}_{xy})^2}{\omega^4}s^2_\omega\right]^{1/2},$$

where s_ω is the standard error on the shear rate

$$s_\omega=\frac{\omega}{r}\left[\frac{1-r^2}{4}\right]$$

(r is the correlation factor) and $s_{\overline{\Pi}_{xy}}$ is the standard error of $\overline{\Pi}_{xy}$ obtained as $s_{\overline{\Pi}_{xy}}=s_{\langle\Pi^\sigma_{xy}\rangle}/\sqrt{n}$ where $s_{\langle\Pi^\sigma_{xy}\rangle}$ is the standard deviation of $\langle\Pi^\sigma_{xy}\rangle$ for a given layer and n is obtained by taking an independent layer every three layers, i.e., $n=(N_L-2)/3$.

In Table IV are reported the results for the shear viscosity. The calculated results must be ascribed to the bulk density ρ_B obtained as the mean on the N_L-2 internal layers. The density of the two boundary layers is different from its "true" value due to the lack of images beyond the Couette walls. It is increased or decreased with respect to the average value depending from the compressibility factor $P/\rho_B kT$.[1] If the compressibility factor is smaller or greater than 1, the bulk density is, respectively, greater or smaller than the average density. This can be seen in Table IV where the compressibility factor is reported together with the bulk density, temperature, and pressure.

The calculated shear viscosities at (ρ_B,P,T) are compared with the experimental values of Ref. 28. For thermodynamical points in the liquid-solid coexistence region it is necessary to extrapolate the experimental data up to these points. Extrapolated results are obtained as follows. We use the data of Ref. 28 at (P,T) together with the empirical law[29]

$$\eta=A\exp(B/T)$$

for the temperature dependence at constant pressure, and

$$\eta=(\partial\eta/\partial P)_T P+C$$

for the pressure dependence at constant temperature. The extrapolated shear viscosity η_{expt} is given by

$$\eta_{\text{expt}}(P_0,T_0)=\eta_{\text{expt}}(P,T)+(\partial\eta/\partial P)_T(P_0-P)+A[\exp(B/T_0)-\exp(B/T)],$$

where P,T are the actual and P_0,T_0 the desired pressure and temperature, A and B are calculated from experimental data at pressure P_0, and $(\partial\eta/\partial P)_T$ is calculated from experimental data at temperature T. For the point at negative pressure the extrapolated shear viscosity corresponds at zero pressure.

The comparison between experimental and computer results gives a good agreement for the test case at lower density, for a shear rate $\omega=0.032$. In the triple-point region the agreement between experimental and computed results is satisfactory up to a shear rate $\omega=0.0082$ for the cases both of 384 and 180 particles. There is no significant dependence on particle number at all shear rates. At higher rates the shear viscosity depends on the applied shear.

C. Nonlinear effects near the triple point

The results obtained for the shear viscosity must be reported at a chosen thermodynamical state, equal for all shear rates, in order to compare with theoretical predictions. We selected the point $\rho_0=0.8442, T_0=0.722$ (near the triple point) and adjusted all results to the chosen point, assuming the same percentage difference between experimental and calculated values. The adjusted values are given by

$$\eta_{\text{ad}}=\frac{\eta^{\text{ad}}_{\text{expt}}}{\eta_{\text{expt}}}\eta,$$

where η and η_{expt} are the computed and experimental shear viscosity in the computed thermodynamical state, and $\eta^{\text{ad}}_{\text{expt}}=22.75$ is the experimental[28] shear viscosity at ρ_0,T_0. In Table IV are also reported the adjusted values.

In Fig. 5 we plot the adjusted shear viscosity versus the shear rate for the cases both of 180 and 384 particles. We also show the fit of the shear dependences for both KGY and Q theories. Table V gives the parameters resulting from both fits and compares these values with experimental and theoretical ones. In Table V we also list the values of the same parameters obtained by fitting data of Refs. 12—14. Our results compare reasonably well with those obtained from the homogeneous shear model.[9]

For the thermodynamical state studied here the theoretical estimates of the parameters predict a much weaker dependence from shear rate. The theoretical estimate for A of KGY is 6×10^3 times greater than the computed one. The theoretical value for Γ, the most important parameter of Q theory is 2×10^2 times greater, For R of Q theory our value is much more near to the predicted Q.

As pointed out previously the local thermodynamical hypothesis is confirmed for all simulated states. Therefore, we do not find any dependence of the pressure and internal potential energy on the shear rate. Finally in Table VI for completeness we list our results together with all other previously obtained results by equilibrium and nonequilibrium MD.

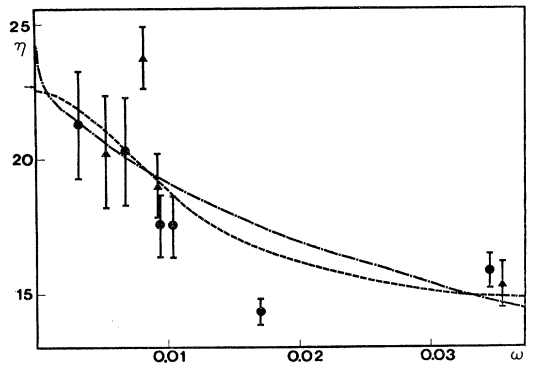

FIG. 5. Shear viscosity adjusted to the point $\rho=0.8442$, $T=0.722$ as a function of the shear rate. ●, $N=384$; ▲, $N=180$; the vertical bar is the standard error; — — — Kawasaki-Gunton-Yamada fit to data; —·—·— Quentrec fit to data. The arrow indicates the experimental result.

VI. CONCLUSIONS

We introduced stochastic boundary conditions to produce stationary shear rates at a fixed boundary temperature in a molecular dynamics system. We analyzed the local thermodynamical properties by dividing the MD system in layers with thickness of the order of the interatomic distance. We applied this technique to study the bulk properties of a system subjected to an applied shear rate. In the bulk, where surface effects are negligible, the local thermodynamical equilibrium holds for all simulated shear rates (up to 1.14×10^{11} sec^{-1}) for different system sizes.

In the boundary layers, where surface effects are dominant, we studied the slip and temperature drop. These effects, well known in the kinetic theory of gases, are important over a region of the order of a mean free path. In our experiment the fluid is dense. Nevertheless we found that these effects are important in a region of the order of the interatomic distance. The validity of the empirical kinetic laws was tested in our computer experiments and found to be in good agreement with the results of simulations.

We computed the shear viscosity from Newton's law, the phenomenological linear law for viscous transport, and looked for its breakdown. In the triple-point region we found this breakdown for shear rates $\omega\geq2.64\times10^{10}$ sec^{-1} and obtained a shear viscosity dependent on the applied shear. We could not detect any dependence of the shear viscosity on the number of particles.

Finally, we compared the calculated shear rate dependence with some theoretical prediction: (i) the mode-mode coupling theory and (ii) the local order theory. Both

TABLE V. Theoretical predictions and computed estimate of the parameters appearing in the theory of KGY (Refs. 20 and 21) and Q (Ref. 23). η_0, extrapolated at $\omega=0$ or experimental shear viscosity; A,R,Γ, fit parameters; σ, standard deviation of the fit. We also show the parameters obtained by fitting all the results of homogeneous shear model (HSM) in Refs. 12—14. All the results are for $T=0.722$, $\rho=0.8442$.

Source	η_0	A	R	Γ	σ
Present work					
KGY fit	24.12±1.78	49.96±14.90			2.01
Q fit	22.61±2.18		0.37±0.08	0.011±0.006	1.94
Experimental	22.75				
Theoretical		0.0088[a] 0.0051[c]	0.53[b]	0.212[b]	
HSM					
KGY fit	22.44±0.37	27.90±1.82			0.89
Q fit	20.25±0.39		0.41±0.03	0.046±0.007	1.04

[a]Reference 20.
[b]Reference 23.
[c]Reference 21.

TABLE VI. Comparison between present results and results from equilibrium and nonequilibrium molecular dynamics methods. The experimental result is also reported. T, temperature; N, particle number; η, shear viscosity and s_η standard error; HSM, homogeneous shear model; FWM, fluid wall model; FDHSM, frequency-dependent HSM; DM, differential method; eq MD, equilibrium molecular dynamics. $\rho=0.8442$.

T	N	$\eta\pm s_\eta$	Source
0.722	180–384	24.12±1.78	KGY fit on present results
0.722	180–384	22.61±2.18	Q fit on present results
0.722	108–324	20.44±1.39	HSM and FWM (Ashurst-Hoover) Ref. 17
0.715	864	20.78±1.04	HSM (Hoover *et al.*) Ref. 17
0.722	108	21.96±0.21	HSM (Evans) Ref. 13
0.722	108	18.71	HSM (Heynes *et al.*) Ref. 14
0.722	108	21.82	FDHSM (Evans) Ref. 13
0.722	256	20.62	HSM with DM (Singer *et al.*) Ref. 19
0.728	108	20.6	EMD (Levesque) Ref. 4
0.715	256	20.2	EMD (Levesque) Ref. 4
0.722	256	18.0±0.7	EMD (Pollock) Ref. 5
0.722	500	22.2±1.4	EMD (Pollock) Ref. 5
0.722	864	26.7	EMD (Levesque) Ref. 4
0.722	864	27.9±2.0	EMD (Levesque *et al.*) Ref. 3
0.722		22.75	Experimental data Ref. 28

theories predict a shear rate dependence much weaker than the one we found. Nonetheless both theories agree with our results in predicting an insignificant breakdown of the local thermodynamical equilibrium. This last result could indicate a weaker dependence on the shear rate of the trace of the stress tensor as compared with its individual components. Work is in progress to clarify these possible effects.

ACKNOWLEDGMENT

We are pleased to thank I. R. Mc Donald for a critical reading of the manuscript.

[1]A. Tenenbaum, G. Ciccotti, and R. Gallico, Phys. Rev. A 25, 2778 (1982).
[2]L. Landau and E. Lifchitz, *Mechanique des Fluides* (Mir, Moscow 1971).
[3]D. Levesque, L. Verlet, and J. Kurkijarvi, Phys. Rev. A 7, 1690 (1973).
[4]D. Levesque (unpublished).
[5]E. L. Pollock (unpublished).
[6]B. L. Holian and D. J. Evans, J. Chem. Phys. 78, 5147 (1983).
[7]W. T. Ashurst and W. G. Hoover, Bull. Am. Phys. Soc. 17, 1196 (1972).
[8]W. T. Ashurst and W. G. Hoover, Phys. Rev. A 11, 658 (1975).
[9]A. W. Lees and S. F. Edwards, J. Phys. C 5, 1921 (1972).
[10]W. T. Ashurst and W. G. Hoover, in *Theoretical Chemistry Advances and Perspectives,* edited by H. Eyring and D. Henderson (Academic, New York, 1975), Vol. 1.
[11]T. Naitoh and S. Ono, J. Chem. Phys. 70, 4515 (1979).
[12]W. T. Ashurst and W. G. Hoover, Phys. Lett. 61A, 175 (1977).
[13]D. J. Evans, Phys. Rev. A 23, 1988 (1981).
[14]D. M. Heyes, J. J. Kim, C. J. Montrose, and T. A. Litovitz, J. Chem. Phys. 73, 3987 (1980).
[15]E. M. Gosling, I. R. McDonald, and K. Singer, Mol. Phys. 26, 1475 (1973).
[16]D. J. Evans, Mol. Phys. 47, 1165 (1982).
[17]W. G. Hoover, D. J. Evans, R. B. Hickman, A. J. C. Ladd, W. T. Ashurst, and B. Moran, Phys. Rev. A 22, 1690 (1980).
[18]G. Ciccotti, G. Jacucci, and I. R. McDonald, J. Stat. Phys. 21, 1 (1979).
[19]K. Singer, J. V. L. Singer, and D. Fincham, Mol. Phys. 40, 515 (1980).
[20]K. Kawasaki and J. D. Gunton, Phys. Rev. A 8, 2048 (1973).
[21]T. Yamada and K. Kawasaki, Prog. Theor. Phys. 53, 111 (1975).
[22]B. Quentrec, J. Mech. (Paris) 20, 449 (1982).
[23]B. Quentrec (private communication).
[24]H. J. M. Hanley and D. J. Evans, J. Chem. Phys. 76, 3225 (1982).
[25]L. Verlet, Phys. Rev. 159, 98 (1967).
[26]J. H. Irving and J. G. Kirkwood, J. Chem. Phys. 18, 817 (1950).
[27]S. Chapman and T. G. Cowling, *The Mathematical Theory of Non-Uniform Gases* (Cambridge University, London, 1960).
[28]*Gas Encyclopaedia* (Elsevier, Amsterdam, 1976).
[29]A. DeBock, W. Grevendonk, and W. Herreman, Physica 37, 227 (1967).